Tunable metamaterial beam with shape memory alloy resonators: Theory and experiment

Vagner Candido de Sousa,[1] David Tan,[2] Carlos De Marqui, Jr.,[1] and Alper Erturk[2,a)]
[1]Department of Aeronautical Engineering, São Carlos School of Engineering, University of São Paulo, São Carlos, SP 13566-590, Brazil
[2]G. W. Woodruff School of Mechanical Engineering, Georgia Institute of Technology, Atlanta, Georgia 30332, USA

(Received 27 July 2018; accepted 17 September 2018; published online 3 October 2018)

We investigate and experimentally validate the concept of bandgap tuning in a locally resonant metamaterial beam exploiting shape memory alloy (SMA) resonators. The underlying mechanism is based on the difference between the martensitic phase (low temperature) and austenitic phase (high temperature) elastic moduli of the resonators, enabling a significant shift of the bandgap for a sufficient temperature change. Experimental validations are presented for a base-excited locally resonant metamaterial beam with SMA resonators following a brief theoretical background. It is shown that the lower bound of the bandgap as well as the bandwidth can be increased by 15% as the temperature is increased from 25 °C to 45 °C for the specific SMAs used in this work for concept demonstration. The change in the bandgap lower bound frequency and its bandwidth is governed by the square root of the fully austenitic to fully martensitic elastic moduli ratio, and it could be as high as 70% or more for other SMAs reported in the literature. *Published by AIP Publishing.* https://doi.org/10.1063/1.5050213

Locally resonant elastic/acoustic metamaterials and resulting finite metastructures with specified boundary conditions enable bandgap formation at wavelengths much longer than the lattice size for applications such as low-frequency vibration/sound attenuation.[1–20] Purely mechanical resonating components are usually not tunable (very few exceptions include bistable configurations[9] that are mechanically tunable to a certain extent), and therefore the bandgap frequency range (i.e., the combination of target frequency and bandwidth) is fixed for a given structure and resonator combination.[16,17]

In this work, we explore a locally resonant metamaterial beam leveraging shape memory alloy (SMA) resonators to enable a tunable bandgap with changing temperature. The concept is based on the mechanism that the elastic moduli of the resonators are altered with temperature as well known from the SMA literature.[21,22] The SMA resonators exhibit martensitic properties at low temperature (e.g., room temperature) to achieve a lower frequency bandgap, which can be shifted to a higher frequency range due to the increased elastic moduli of the resonators associated with the austenitic phase.

Consider the temperature-related SMA phase transformation kinetics[21] in a low-stress case such that only the low- and high-temperature phases take place (i.e., the self-accommodated/twinned martensitic phase and the austenitic phase, respectively). The typical four transition temperatures of SMAs[21,22] are considered: the martensite finish (M_f), the martensite start (M_s), the austenite start (A_s), and the austenite finish (A_f), in the ascending order. Assume an internal variable, the martensitic fraction (denoted by ξ), to represent the amount of phase transformation in the SMA ($\xi = 1$ in the fully martensitic phase while $\xi = 0$ in the fully austenitic phase). Using Brinson's model,[21] the martensitic fraction at low temperature ($M_f \leq T \leq M_s$, where T is the SMA temperature) can be given by

$$\xi = \frac{1-\xi_0}{2}\left[\cos\left(\pi\frac{T-M_f}{M_s-M_f}\right)+1\right], \tag{1}$$

where subscript 0 denotes the value at the onset of the current phase transformation. At high temperature ($A_s \leq T \leq A_f$), the martensitic fraction is

$$\xi = \frac{\xi_0}{2}\left[\cos\left(\pi\frac{T-A_s}{A_f-A_s}\right)+1\right]. \tag{2}$$

The SMA elastic modulus can be defined in terms of the martensitic fraction as $E(\xi) = E_A + \xi(E_M - E_A)$, where E_M is the fully martensitic modulus and E_A is the fully austenitic modulus. The phase transformation (evolution of the martensitic fraction with temperature) and the corresponding elastic moduli for an arbitrary SMA element are depicted in Fig. 1.

Next, an Euler-Bernoulli type locally resonant metamaterial beam model is briefly reviewed based on the theory by Sugino *et al.*[16,17] Consider an undamped thin cantilevered beam with flexural rigidity EI, mass per unit length m, and length L, as shown in Fig. 2, under the excitation of the transverse base displacement $w_b(t)$. The relative transverse displacement is denoted by $w(x, t)$, such that the absolute displacement is $w_{\text{abs}}(x, t) = w_b(t) + w(x, t)$. The locally resonant metamaterial beam has S undamped resonators attached to the beam, at locations x_j, with masses m_j, and relative displacements u_j, for $j = 1, 2, \ldots, S$. The linear resonators have stiffnesses k_j and natural frequencies $\omega_{a,j}^2 = k_j/m_j$, which are typically assumed to be identical (see Ref. 16 for details). Furthermore, damping is neglected at this point without loss

a)Author to whom correspondence should be addressed: alper.erturk@me.gatech.edu.

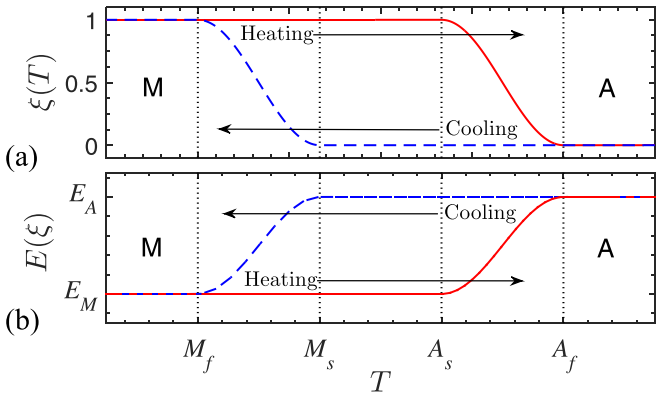

FIG. 1. (a) Evolution of the martensitic fraction for a heating/cooling cycle of an arbitrary SMA element and (b) the corresponding change in the SMA elastic modulus, where M is the fully martensitic phase and A is the fully austenitic phase.

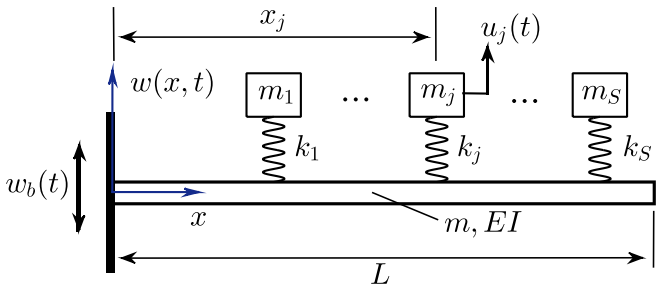

FIG. 2. Schematic of a cantilevered locally resonant metamaterial beam under base excitation.

of generality, and modal damping can be added at a later stage. The governing equations of motion can be modified for SMA resonators by including the dependence of the elastic moduli of the resonators on the martensitic fraction such that $\omega_{a,j} = \omega_{a,j}(\xi)$ (details can be found in Ref. 23).

Using an expansion with N terms and employing the corresponding plain beam mode shapes[24] yield

$$w(x,t) = \sum_{k=1}^{N} \phi_k(x)\eta_k(t), \tag{3}$$

where ϕ_k is the kth mode shape and η_k is the corresponding modal weighting. The governing equations in modal coordinates for the metamaterial beam with SMA resonators can be given by[16,23]

$$\sum_{i=1}^{N}\left[\delta_{ik} + \sum_{j=1}^{S}\hat{m}_j\phi_i(x_j)\phi_k(x_j)\right]\ddot{\eta}_i(t) + \sum_{j=1}^{S}\hat{m}_j\phi_k(x_j)\ddot{u}_j(t) + \omega_k^2\eta_k(t) = -\ddot{w}_b(t)\left(\int_0^L \phi_k(x)dx + \sum_{j=1}^{S}\hat{m}_j\phi_k(x_j)\right), \tag{4}$$

$$\ddot{u}_j(t) + \omega(\xi)_{a,j}^2 u_j(t) + \sum_{i=1}^{N}\ddot{\eta}_i(t)\phi_i(x_j) = -\ddot{w}_b(t), \tag{5}$$

where δ_{ik} is the Dirac delta function and $\hat{m}_j = m_j/(mL)$ is the jth normalized resonator mass. The free indices k and j go from 1 to N and 1 to S, respectively ($i = 1, 2, \ldots, N$ is the coupling between modes).

Defining ω as the excitation frequency and ω_t as the target frequency of the resonators (the lower bound of the bandgap), the beam with resonators exhibit no resonances in the range $\omega_t < \omega < \omega_t\sqrt{1+\mu}$, which defines the limits of the bandgap,[16] where μ is the mass ratio. The bandwidth of the bandgap is, therefore, $\Delta\omega = \omega_t\left(\sqrt{1+\mu} - 1\right)$. The bandgap width of a metamaterial beam with SMA resonators is bounded within $\Delta\omega^M = \omega_t^M\left(\sqrt{1+\mu} - 1\right)$ and $\Delta\omega^A = \omega_t^A\left(\sqrt{1+\mu} - 1\right)$ as the SMAs change from the martensitic phase (with $\omega_{a,j} = \omega_t = \omega_t^M$) to the austenitic phase (with $\omega_{a,j} = \omega_t = \omega_t^A$), respectively. Rearranging these equations, the increase in the bandgap width achieved when the SMA resonators change from the martensitic phase to the austenitic phase is $\Delta\omega^A/\Delta\omega^M = \sqrt{E_A/E_M}$. Note that the mass ratio (μ) remains the same; therefore, $\Delta\omega^M/\omega_t^M = \Delta\omega^A/\omega_t^A$.

Experiments were performed for concept demonstration and model validation. SMA beams with $A_f \approx 45\,^\circ$C (denoted as "standard temperature" by the manufacturer, Kellogg's Research Labs) were used for the experiments. The SMA beams are 132.1 mm long, 12.5 mm wide, and 0.75 mm thick, with a mass per length of 0.0598 kg/m and a density of 6351 kg/m^3. The electrical resistance of each SMA beam measured at room temperature was 0.2 Ω. Due to the low electrical resistance, sufficient heat generation through the Joule effect would require a large electrical current; as an alternative, hot air provided by a heat gun was employed for thermal stimulation of the SMA beams. Temperatures were measured both with an infrared thermometer and a thermal camera. The transverse vibrations of the beams were measured by using a Polytec OFV-505 laser Doppler vibrometer (LDV).

For the identification of the SMA elastic moduli, free vibration tests were conducted at different temperatures between 0 °C and 100 °C. In these preliminary characterization experiments, a 100 mm long cantilevered SMA beam without a tip mass was considered. Small initial displacements were applied to the SMA beam to ensure that no stress-induced phase transformation took place and linear elastic behavior was observed. The free oscillation frequency below room temperature was 33.2 Hz, while at room temperature it was 32.4 Hz. The slight decrease in free vibration frequency when the SMA temperature changed from $T \ll T_\infty$ to $T \approx T_\infty$ is possibly an effect of the R-phase, a trigonal lattice with a martensitic nature that can be attributed to composition inhomogeneity.[25,26] At temperatures greater than 45 °C, the oscillation frequency increased to 41.1 Hz. The damping ratio values were estimated (by the logarithmic decrement method) as 0.0072 and 0.0043 for the low- and high-temperature cases, respectively.

The SMA characterization test results are summarized in Fig. 3. The free vibration frequency is shown in Fig. 3(a) and the damping ratio is shown in Fig. 3(b). Solid markers (for $T \le T_\infty$ and $T \ge A_f$) represent experimental data. Markers for $T_\infty < T < A_f$ were numerically obtained by using Eqs. (1) and (2) (after calculating the SMA elastic moduli). Figure 4(a) displays the free vibration responses of the SMA

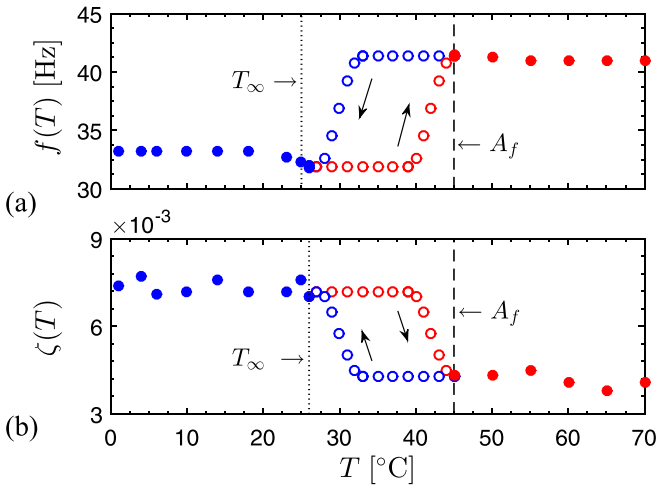

FIG. 3. (a) Oscillation frequency and (b) damping ratio for a cantilevered SMA beam with $A_f \approx 45\,^\circ$C at several different temperatures. Solid markers represent experimental data.

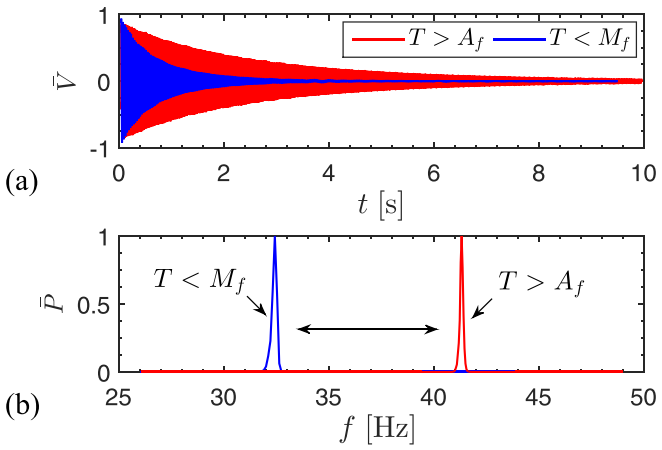

FIG. 4. (a) Experimental free vibration response and (b) oscillation frequency data at two different temperatures (low temperature in blue and high temperature in red). Graphs are normalized to have unity peak value.

beam at room temperature (in blue) and above the A_f temperature (in red), and the respective frequency contents are shown in Fig. 4(b).

The flexural rigidity for the individual SMA beams was obtained as $E_M I = 0.020\,\text{Nm}^2$ and $E_A I = 0.031\,\text{Nm}^2$, and the moment of inertia was $I = 4.3 \times 10^{-13}$ m^4. The resulting martensitic modulus (for $T \leq M_f$) was $E_M = 45$ GPa and the austenitic modulus (for $T \geq A_f$) was $E_A = 73$ GPa. However, several SMA beams were tested and a number of them exhibited an austenitic modulus as low as 60 GPa. With the elastic moduli experimentally identified, the SMA beams were then employed to construct the metamaterial beam. A cantilevered beam forms the main structure (6061 aluminum alloy, with an elastic modulus of 68.9 GPa, a density of 2700 kg/m^3, a width of 25.4 mm, a thickness of 1.59 mm, and an exposed length of 248 mm). Point masses (25.4 mm long, 12.7 mm wide magnets) were evenly distributed on the main beam for the attachment of five SMA beam resonators (127 mm long, 12.7 mm wide SMA beams). The attachment masses (total of 61 g) do not contribute to the mass of the resonators, but affect the resonant frequencies and the mass ratio of the metamaterial beam (hence the bandwidth of the bandgap). After attaching the SMA beams to the main aluminum cantilever, the overhang length of the SMA resonator beams on each side was 50 mm, as shown in Fig. 5 along with the setup components. An infrared capture of the metamaterial beam at high-temperature shows that all SMAs are above the A_f temperature. Although the temperature is not uniform, it is deemed acceptable (emissivity was set to 0.95). A long-stroke shaker (APS Dynamics Inc.) was used for base excitation of the structure and the LDV measured vibrations at the tip of the metamaterial beam. The bandgap associated with the martensitic phase of the SMAs (when at room temperature) was centered around the second resonant frequency of the plain beam (that contained the point masses used in attaching the SMAs to the aluminum beam) by using 5.65 g tip masses on the SMA resonators. The resulting mass ratio (μ) was around 0.7, yielding a bandwidth of 15 Hz for the bandgap (and $\Delta\omega/\omega_t = 0.3$).

The metamaterial beam was first tested at room temperature so that the SMAs were in the fully martensitic phase. At constant temperature and small deformations of the SMAs (to ensure no stress-induced phase transformation), the SMA resonators behaved as ordinary linear resonators. As mentioned previously, $\sqrt{E_A/E_M}$ is the change in the target frequency (ω_t) achieved when the SMA resonators switch from the martensitic phase to the austenitic phase. For the SMAs under consideration, the target frequency is expected to increase around 20% when the temperature of the SMAs increases from $T \leq M_f$ (which includes room temperature) up to $T \geq A_f$ since $\sqrt{E_A/E_M} \approx 1.2$. At or below room temperature, $\omega_t = \omega_t^M$ since $M_f \approx 25\,^\circ$C. At temperatures greater than A_f (around 45 °C), $\omega_t = \omega_t^A \approx 1.2\omega_t^M$.

Figure 6 shows the transmissibility frequency response functions (FRFs) of the metamaterial beam with SMA

FIG. 5. Experimental setup to test a metamaterial beam with SMA resonators (left). Infrared picture during an arbitrary high-temperature test (right).

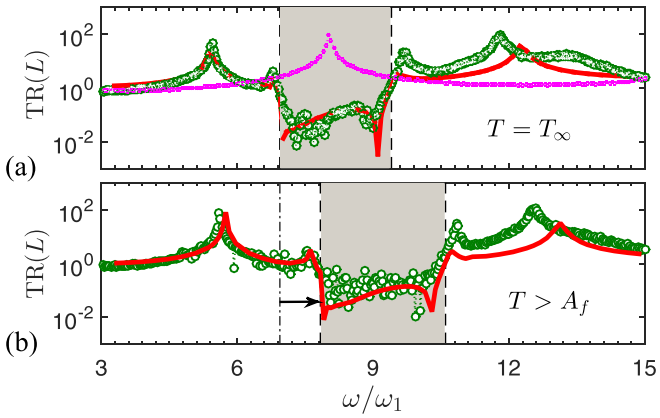

FIG. 6. Bandgap tuning in the locally resonant metamaterial beam with SMA resonators: transmissibility FRFs (a) at room temperature in the fully martensitic phase (showing also the plain beam case in magenta) and (b) at a temperature above 45 °C in the fully austenitic phase. Green lines with markers represent the experimental data. Continuous red lines are model simulations.

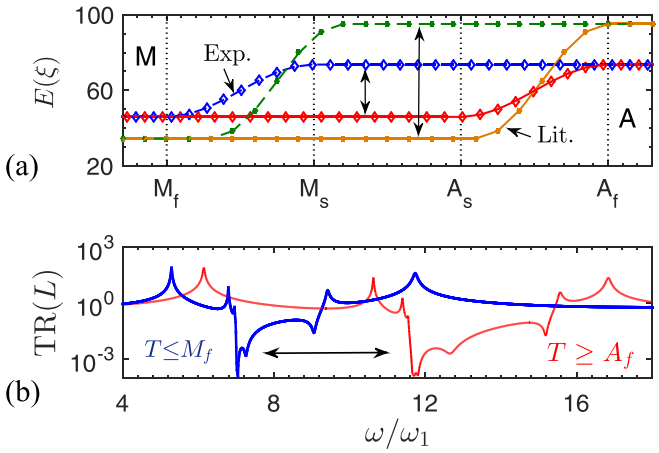

FIG. 7. (a) Representation of the elastic moduli of the SMA beams tested in this work (lines with larger markers) and of a nitinol SMA reported in the literature[21] (lines with smaller markers in orange and green stand for the heating and cooling stages, respectively) and (b) the predicted bandgap tuning for the nitinol properties reported in the latter scenario.

resonators. In these graphs, $\mathrm{TR}(L) = |\bar{w}_{\mathrm{abs}}(L)/\bar{w}_b|$ is the transmissibility at the free end of the main beam (tip displacement to base displacement ratio) in the magnitude form, while the frequency axis is normalized with respect to the first resonant frequency of the metamaterial beam (6.7 Hz). The transmissibility FRFs for the two distinct limiting cases are shown in the figure. The bandgap at a lower frequency range was obtained for the SMAs at room temperature (in the fully martensitic phase) as shown in Fig. 6(a) along with the plain beam frequency response (exhibiting the mode being targeted). As displayed in Fig. 6(b), bandgap at a higher frequency range was obtained for the SMAs at high temperature (above 45 °C, in the fully austenitic phase). The target frequency increased by around 15% from the low-temperature case to the high-temperature case, changing from 46 Hz to 53 Hz. The bandwidth increased by the same ratio since $\Delta\omega/\omega_t$ (controlled by the mass ratio, μ) remains the same.

While the results in Fig. 6 validate the concept and model for SMA-based bandgap tuning with temperature, the amount of bandgap shift was limited by the particular SMAs used in this work. It is worth mentioning that a number of SMAs were reported in the existing literature which exhibit a factor of 2–3 increase in the elastic modulus from the martensitic phase to the austenitic phase.[21,22] In such cases, an increase of 40%–70% in the bandgap could be expected. To put it in context, the target frequency of 46 Hz (the lower bound of the bandgap) could be increased to 78 Hz with such SMA resonators, and the bandgap width would increase by the same factor (a numerical simulation of this scenario is shown in Fig. 7). Moreover, this increase in the elastic modulus could take place for roughly the same increase in temperature reported in this work (as low as 20 °C between the martensitic and austenitic phases). The advantage of using SMA resonators is further supported by the possibility of a metamaterial with self-tuning capabilities by exploiting the environmental temperature change[27] since SMA transition temperatures can be tailored through alloy composition and heat treatment.[28,29]

In summary, we demonstrated bandgap tuning in a locally resonant metamaterial beam with SMA resonators. The concept leveraged changing the temperature to alter the elastic moduli of the resonators by moving from the fully martensitic to the fully austenitic phase. As demonstrated via our modeling framework, and validated experimentally, the target frequency of the resonators (i.e., the lower bound of the bandgap) as well as the locally resonant bandgap width increases by the factor of $\sqrt{E_A/E_M}$. The amount of temperature change required can be rather low (e.g., 20 °C), which can be achieved easily and potentially by environmental temperature change in certain applications.

This work was supported by the São Paulo Research Foundation (FAPESP) (Grant Nos. 2017/08467-6 and 2015/26045-6) and by the Air Force Office of Scientific Research (AFOSR) Grant No. FA9550-15-1-0397.

[1]Z. Liu, X. Zhang, Y. Mao, Y. Y. Zhu, Z. Yang, C. T. Chan, and P. Sheng, Science **289**, 1734 (2000).
[2]K. M. Ho, C. K. Cheng, Z. Yang, X. X. Zhang, and P. Sheng, Appl. Phys. Lett. **83**, 5566 (2003).
[3]Z. Yang, J. Mei, M. Yang, N. H. Chan, and P. Sheng, Phys. Rev. Lett. **101**, 204301 (2008).
[4]M. Oudich, M. Senesi, M. B. Assouar, M. Ruzzene, J.-H. Sun, B. Vincent, Z. Hou, and T.-T. Wu, Phys. Rev. B **84**, 165136 (2011).
[5]Y. Xiao, J. Wen, and X. Wen, J. Phys. D: Appl. Phys. **45**, 195401 (2012).
[6]E. Baravelli and M. Ruzzene, J. Sound Vib. **332**, 6562 (2013).
[7]S. Chen, G. Wang, J. Wen, and X. Wen, J. Sound Vib. **332**, 1520 (2013).
[8]H. Peng and P. F. Pai, Int. J. Mech. Sci. **89**, 350 (2014).
[9]P. Wang, F. Casadei, S. Shan, J. C. Weaver, and K. Bertoldi, Phys. Rev. Lett. **113**, 014301 (2014).
[10]R. Zhu, X. N. Liu, G. K. Hu, C. T. Sun, and G. L. Huang, J. Sound Vib. **333**, 2759 (2014).
[11]M. Nouh, O. Aldraihem, and A. Baz, J. Sound Vib. **341**, 53 (2015).
[12]C. Xu, F. Cai, S. Xie, F. Li, R. Sun, X. Fu, R. Xiong, Y. Zhang, H. Zheng, and J. Li, Phys. Rev. Appl. **4**, 034009 (2015).
[13]G. Hu, L. Tang, A. Banerjee, and R. Das, J. Vib. Acoust. **139**, 011012 (2016).
[14]J. Li, X. Zhou, G. Huang, and G. Hu, Smart Mater. Struct. **25**, 045013 (2016).
[15]K. H. Matlack, A. Bauhofer, S. Krödel, A. Palermo, and C. Daraio, Proc. Natl. Acad. Sci. **113**, 8386 (2016).
[16]C. Sugino, S. Leadenham, M. Ruzzene, and A. Erturk, J. Appl. Phys. **120**, 134501 (2016).

[17]C. Sugino, Y. Xia, S. Leadenham, M. Ruzzene, and A. Erturk, J. Sound Vib. **406**, 104 (2017).
[18]C. Sugino, S. Leadenham, M. Ruzzene, and A. Erturk, Smart Mater. Struct. **26**, 055029 (2017).
[19]A. Casalotti, S. El-Borgi, and W. Lacarbonara, Int. J. Non-Linear Mech. **98**, 32 (2018).
[20]G. Hu, L. Tang, and R. Das, J. Appl. Phys. **123**, 055107 (2018).
[21]L. Brinson, J. Intell. Mater. Syst. Struct. **4**, 229 (1993).
[22]D. C. Lagoudas, *Shape Memory Alloys* (Springer US, Boston, MA, 2008), Vol. 1.
[23]V. Candido de Sousa, C. Sugino, C. De Marqui Junior, and A. Erturk, J. Appl. Phys. **124**, 064505 (2018).
[24]L. Meirovitch, *Principles and Techniques of Vibration* (Prentice Hall, Upper Saddle River, NJ, 1997), p. 694.
[25]S. Saedi, A. S. Turabi, M. Taheri Andani, C. Haberland, H. Karaca, and M. Elahinia, J. Alloys Compd. **677**, 204 (2016).
[26]S. Saedi, A. S. Turabi, M. T. Andani, N. S. Moghaddam, M. Elahinia, and H. E. Karaca, Mater. Sci. Eng.: A **686**, 1 (2017).
[27]J. H. Mabe, F. T. Calkins, and R. T. Ruggeri, Proc. SPIE **6525**, 65251C (2007).
[28]J. Frenzel, E. P. George, A. Dlouhy, C. Somsen, M. F. X. Wagner, and G. Eggeler, Acta Mater. **58**, 3444 (2010).
[29]M. H. Elahinia, M. Hashemi, M. Tabesh, and S. B. Bhaduri, Prog. Mater. Sci. **57**, 911 (2012).